Electronic Supplementary Material (ESI) for CrystEngComm.

Flux-assisted polytypism in the $[Na_2Cl]GaQ_2$ heterolayered salt-inclusion chalcogenide family

Anna A. Berseneva,[a] Vladislav V. Klepov,[b] Hunter B. Tisdale,[a] Hans-Conrad zur Loye[a]*

[a] Department of Chemistry and Biochemistry, University of South Carolina, Columbia, South Carolina, 29208, USA
[b] Department of Chemistry, University of Georgia, Athens, Georgia, 30602, USA

*Corresponding author. E-mail: zurloye@mailbox.sc.edu

Physical Measurements

Single-Crystal X-ray Diffraction (SCXRD). SCXRD data were collected at 299(2)–302(2) K on a Bruker D8 QUEST diffractometer equipped with an Incoatec IμS 3.0 microfocus radiation source (MoKα, λ = 0.71073 Å) and a PHOTON II area detector. The crystals were mounted on a microloop using immersion oil. The raw data reduction and absorption corrections were performed using SAINT and SADABS programs.[1, 2] Initial structure solutions were obtained with SHELXS-2017 using direct methods and Olex2 GUI.[3] Full-matrix least-square refinements against $|F|^2$ were performed with SHELXL software.[4] The crystallographic data and results of the diffraction experiments are summarized in Tables S1 and S4.

Powder X-ray Diffraction (PXRD). PXRD data were collected on a Bruker D2 PHASER diffractometer using CuKα radiation (λ = 1.5418 Å) over the 2θ range 5–65 ° with a step size of 0.02° for 30 minutes. For high-temperature PXRD, patterns were collected on a Rigaku SmartLab Diffractometer in transmission geometry using a MoKα rotating anode (45 kV, 200 mA; λ = 0.71073 Å) equipped with an Anton Parr HTK1200N heating stage. A powder sample of $[Na_2Cl]GaS_2$ was loaded in a quartz capillary with an outer diameter of 1.0 mm and a wall thickness of 0.01mm and sealed. The sample was heated *in situ* in a hot stage that allowed rotation of the capillary during heating. Data were collected over the 2θ range 4–35 ° in 0.01° steps for 30 minutes. An initial PXRD pattern was collected at 25 °C and 100°C, and then the sample was heated at a rate of 10 °C/min from 100 °C to 400 °C, collecting data every 50 °C, then with the same heating rate; the sample was heated to 500 °C, collecting data every 25 °C, and finally to 650 °C, collecting data every 10 °C. The diffraction patterns were analyzed using the Rigaku SmartLab Studio II software.

Energy Dispersive Spectroscopy (EDS). EDS was performed directly on crystals mounted on an SEM stub with carbon tape. Quantitative elemental analysis was carried out using a Tescan Vega-3 SEM instrument equipped with a Thermo EDS attachment. The SEM was operated in the low-vacuum mode with a 30 kV accelerating voltage and a 120 s accumulating time. The EDS results are summarized in Table S3 and Figures S5–S8, S10, and S11.

Thermogravimetric Analysis (TGA). Thermogravimetric and differential thermal analysis (TGA/DTA) measurements were performed on polycrystalline powder samples using a SDT Q600 Thermogravimetric Analyzer and an alumina pan as the sample holder. Samples were heated from room temperature to the target temperature (700 °C or 900 °C) at 10 °C/min under a flow of nitrogen gas (100 mL/min), and the resulting powders were analyzed by PXRD for phase identification post heating.

UV-vis Spectroscopy. UV-vis spectra were recorded using a Perkin-Elmer lambda 35 scanning spectrophotometer. The spectrophotometer was operated in diffuse reflectance mode and was equipped with an integrating sphere. Reflectance data were converted internally to absorbance *via* the Kubelka-Munk function. Spectra were recorded in the 200–900 nm range.

Fourier-Transform Infrared (FTIR) Spectroscopy

Vibrational spectra over the range of 4000–650 cm^{-1} were recorded using a PerkinElmer Spectrum 100 FT-IR spectrometer equipped with a diamond attenuated total reflectance (ATR) attachment. Final infrared (IR) spectra consist of 20 total averaged scans.

Computational Details. All DFT calculations were carried out using the Vienna Ab-initio Simulation Package (VASP)[5, 6] utilizing the Projector Augmented-Wave (PAW) potential.[7]

The PBE parametrization of the generalized gradient approximation (GGA) to the exchange-correlation functional was used for the calculations.[8] We used the following potentials of the constituent elements: Li_sv ($1s^2\ 2s^1$), F ($2s^2\ 2p^5$), Na_pv ($2p^6\ 3s^1$), S ($3s^2\ 3p^4$), Cl ($3s^2\ 3p^5$), K_sv ($3s^2\ 3p^6\ 4s^1$), Ga ($3s^2\ 3p^1$), and Br ($4s^2\ 4p^5$). All compounds were structurally relaxed (volume, cell shape, and atomic positions) starting from their experimentally known crystal structures, where available, following the DFT settings in the OQMD.[9, 10] The threshold for energy convergence was set to 10^{-6} eV. The relaxed geometries of the $[A_2X]GaS_2$ compounds preserve the $P4_2/nmc$ space group during structure relaxation. For $[Na_2Cl]GaS_2$ composition, geometry relaxation was also done for orthorhombic polymorph while keeping the *Cmcm* space group. The energy cutoff for the DFT calculations was set to 520 eV for static calculations. The optimized lattice constants agree very well (error < 1.2%) with the experimental values (Table S5).

In relation to the current experimental work, we assessed the T = 0 K thermodynamic stabilities of the $[A_2X]GaS_2$ compounds. We calculated their formation energies, $\Delta H_f^{0K} = E(\sigma) - \sum_i n_i \mu_i$ (Table S5), where E is the DFT-calculated total energy at 0 K for a compound σ, n_i is the fraction of the i-th element with chemical potential μ_i. Utilizing the formation energies of these compositions and all other compounds that are present in each quaternary phase space; we constructed the quaternary convex hull for $[A_2X]GaS_2$ in the OQMD that allowed to estimated decomposition energies (Table S5). Typical decomposition of $[A_2X]GaS_2$ leads to AX and $AGaS_2$. Only $[Na_2Cl]GaS_2$ and $[Na_2Br]GaS_2$ compounds demonstrated stability in the *A*–*X*–Ga–S landscape since they have positive decomposition enthalpies estimated by convex hull constriction.

Synthesis

Materials. The following materials were used as received without further purification: S (Fisher Scientific, 99%), Ga (BTC, 99.999%), Se (Alfa Aesar, 99.999%), Na_2S (Alfa Aesar, 95%), NaCl (Fisher Chemical, 99.9%), NaBr (BTC, 99.0%), NaI (Fisher Chemical, 99.9%), dimethylformamide (DMF, Sigma-Aldrich, 99.8%), and acetone (BDH, 99.5%). Synthesis of Na_2Se was performed using a reported procedure.[11] For all mentioned reactions, masses of the reagents were mixed inside a silica tube. Typically, the silica tube was flame sealed under a vacuum of $<10^{-4}$ Torr. The sealed tube was placed vertically into a programmable box furnace with the corresponding temperature profile. Once at room temperature, the tube was cut open, and the reaction products were put into a beaker filled with deionized (DI) water or DMF.

$[Na_2Cl]GaQ_2$ (Q = S and Se). The starting reagents, Ga (0.0540 g), Q, Na_2Q in a 1:2:1 molar ratio, and NaCl/NaI flux (0.054/0.159 g) were used to grow single crystals of $[Na_2Cl]GaQ_2$. The furnace with the tube was ramped up to 650 °C in 3 or 5 h, held at this temperature for 5 or 24 h, and then cooled to 450 or 250 °C at a cooling rate of 40 or 5 °C/h for S- and Se-based compounds, respectively. After the reaction and work up in water were complete, the final product was filtered and washed with distilled water and acetone. Single crystals of $[Na_2Cl]GaQ_2$ were placed in immersion oil and mounted for SCXRD. The PXRD pattern for the bulk sample matches the simulated pattern obtained from SCXRD (Figures S13 and S16). The PXRD pattern for $[Na_2Cl]GaS_2$ contained minor $NaGaS_2 \cdot H_2O$ impurity (Figure S13). This correlates with a colling rate chosen for sulfide formation (40 °C/h) versus selenide (5 °C/h),

resulting in precipitation from the flux of $NaGaS_2$, which converted to $NaGaS_2 \cdot H_2O$ after work-up in water. For phase pure $[Na_2Cl]GaS_2$ synthesis, the amount of flux was doubled to 0.108 g and 0.318 g of NaCl and NaI, respectively. The furnace with the tube was ramped up to 650 °C in 5 h, held at this temperature for 48 h, and then cooled to 200 °C at a cooling rate of 5 °C/h. The PXRD pattern for the bulk sample matches the simulated pattern obtained from SCXRD (Figure S14). We also attempted to collect the PXRD pattern for tetragonal polymorph $[Na_2Cl]GaS_2$ only; for that, we isolated *t*-$[Na_2Cl]GaS_2$ single crystal, crashed it, and collected data on the resulting powder using phi scan in SC-XRD instrument (Figure S15) that matches well the simulated pattern of *t*-$[Na_2Cl]GaS_2$.

Na_2GaSe_3 and $Na_4Ga_2Se_5$. In an attempt to obtain $[Na_2Br]GaSe_2$ single crystals, we grew crystals of Na_2GaSe_3 and $Na_4Ga_2Se_5$ instead. The starting reagents, Ga (0.0540 g), Se (0.1230 g), Na_2Se (0.096 g) in a 1:2:1 molar ratio, and NaBr/NaI flux (0.095/0.208 g) were used to obtain single crystals of Na_2GaSe_3 and $Na_4Ga_2Se_5$. The furnace with the tube was ramped up to 650 °C in 5 h, held at this temperature for 24 h, and then cooled to 250 °C at a cooling rate of 10 °C/h. After the reaction and work up in DMF were complete, the final product was filtered and washed with acetone. The product was placed in immersion oil where the pink rod Na_2GaSe_3 and the colorless block $Na_4Ga_2Se_5$ single crystals were isolated and mounted for SCXRD. PXRD pattern for the bulk sample consisted of multiple phases: Na_2GaSe_3, $Na_4Ga_2Se_5$, and $NaGaSe_2 \cdot xH_2O$,[12] and no further attempts were made to obtain the phase pure samples.

X-ray Crystal Structure Determination

***o*-$[Na_2Cl]GaS_2$.** The compound crystallizes in the orthorhombic crystal system, space group *Cmcm*. The asymmetric unit consists of seven Na atoms, two Cl halogens, two Ga atoms, and five S chalcogens. The largest residual electron density peak in the final difference map is 0.58e-/Å^3, located 0.68 Å from Na6. The crystallographic data and results of the diffraction experiments are summarized in Table S1.

***o*-$[Na_2Cl_{0.9}I_{0.1}]GaSe_2$.** The compound crystallizes in the orthorhombic crystal system, space group *Cmcm*. The asymmetric unit consists of seven Na atoms, two Cl and two I halogens, two Ga atoms, and five Se chalcogens. There is a disorder between Cl and I for both Cl crystallographic sites. Positions and thermal ellipsoids for Cl1 and I1, as well as for Cl2 and I2 pairs, were fixed using EXYZ and EADP commands. Occupancies of Cl and I were linked with FVAR command; thus, total site occupancy is equal to 1. Cl1 and Cl2 occupancies were refined to 0.894(5) and 0.921(4), respectively. The largest residual electron density peak in the final difference map is 1.28 e-/Å^3, located 1.48 Å from Ga2. The crystallographic data and results of the diffraction experiments are summarized in Table S1. Precession images for (*h*0*l*) planes generated for the orthorhombic *C* Bravais lattice demonstrated superstructure peaks of low intensity, however, attempts to solve this structure in orthorhombic *C* lattice with double *a* parameter, i.e., 15.194 Å vs. 7.597 Å, that accounts for the superstructure, did not result in a reasonable structure model.

***t*-$[Na_2Cl]GaS_2$.** The compound crystallizes in the orthorhombic crystal system, space group $P4_2/nmc$. The asymmetric unit consists of three Na atoms, one Cl halogen, one Ga atom, and

three S chalcogens. The largest residual electron density peak in the final difference map is 1.23e-/Å^3, located 1.85 Å from Na2. The crystallographic data and results of the diffraction experiments are summarized in Table S1.

***t*-[$Na_2Cl_{0.9}I_{0.1}$]$GaSe_2$.** The compound crystallizes in the orthorhombic crystal system, space group *P*4$_2$*/nmc*. The asymmetric unit consists of three Na atoms, one Cl and one I halogen, one Ga atom, and three Se chalcogens. There is a disorder between Cl and I. Positions and thermal ellipsoids for Cl1 and I1 were fixed using EXYZ and EADP commands. Occupancies of Cl and I were linked with FVAR command; thus, total site occupancy is equal to 1. Cl1 occupancy was refined to 9075(19). The largest residual electron density peak in the final difference map is 0.97 e-/Å^3, located 0.80 Å from Na1. The crystallographic data and results of the diffraction experiments are summarized in Table S1.

Na_2GaSe_3. The compound crystallizes in the monoclinic crystal system, space group *C*2/*c*. The asymmetric unit consists of three Na atoms, one Ga atom, and three Se chalcogens. The largest residual electron density peak in the final difference map is 0.70e-/Å^3, located 0.98 Å from Na1. The crystallographic data and results of the diffraction experiments are summarized in Table S4.

$Na_4Ga_2Se_5$. The compound crystallizes in the monoclinic crystal system, space group *P*2$_1$/*c*. The asymmetric unit consists of four Na atoms, two Ga atoms, and five Se chalcogens. The largest residual electron density peak in the final difference map is 0.57e-/Å^3, located 1.36 Å from Ga2. The crystallographic data and results of the diffraction experiments are summarized in Table S4.

Table S1. Crystallographic data for *o*-$[Na_2Cl]GaS_2$, *t*-$[Na_2Cl]GaS_2$, *o*-$[Na_2Cl_{0.9}I_{0.1}]GaSe_2$, and *t*-$[Na_2Cl_{0.9}I_{0.1}]GaSe_2$.

compound	*o*-$[Na_2Cl]GaS_2$	*t*-$[Na_2Cl]GaS_2$	*o*-$[Na_2Cl_{0.9}I_{0.1}]GaSe_2$	*t*-$[Na_2Cl_{0.9}I_{0.1}]GaSe_2$
empirical formula	Na_2ClGaS_2	Na_2ClGaS_2	$Na_2Cl_{0.91}I_{0.09}GaS_2$	$Na_2Cl_{0.91}I_{0.09}GaS_2$
formula weight	215.27	215.27	317.53	317.53
temperature, K	299.85	301.61	299.85	299.08
crystal system	orthorhombic	tetragonal	orthorhombic	tetragonal
space group	*Cmcm*	$P4_2/nmc$	*Cmcm*	$P4_2/nmc$
a, Å	7.2885(2)	7.2850(2)	7.597(2)	7.5821(2)
b, Å	39.4434(10)	7.2850(2)	41.001(11)	7.5821(2)
c, Å	7.2884(2)	19.7163(5)	7.583(2)	20.4761(5)
α, °	90			
β, °				
γ, °				
volume, $Å^3$	2095.29(10)	1046.37(6)	2362.0(11)	1177.13(7)
Z	16	8	16	8
ρ_{calc}, g/cm^3	2.73	2.733	3.572	3.583
crystal size, mm^3	0.05 × 0.04 × 0.02	0.8 × 0.1 × 0.08	0.2 × 0.05 × 0.05	0.1 × 0.07 × 0.02
2*Θ* range for data collection, °	5.684 to 64.978	5.962 to 55.944	5.454 to 55	5.73 to 59.972
index ranges	$-11 \le h \le 11$, $-59 \le k \le 59$, $-11 \le l \le 11$	$-9 \le h \le 9$, $-9 - k \le 9$, $-26 \le l \le 26$	$-9 \le h \le 9$, $-53 \le k \le 53$, $-9 \le l \le 9$	$-10 \le h \le 10$, $-9 \le k \le 10$, $-28 \le l \le 28$
reflections collected	66207	48407	45040	33459
data/restraints/ parameters	2158/0/80	736/0/40	1557/0/83	987/0/42
Goodness-of-fit on F^2	1.078	1.132	1.145	1.171
R_1/wR_2 [I>=2σ (I)], %	1.34/2.95	1.90/4.91	4.02/11.21	1.66/3.44
R_1/wR_2 [all data], %	1.78/3.20	2.07/5.20	4.39/11.73	3.10/4.60
largest diff. peak/hole, e $Å^{-3}$	0.58/–0.64	1.23/–0.52	1.28/–1.11	0.97/–0.66
R_{int}, %	3.45	7.36	5.08	6.42

Table S2. Selected interatomic distances for *o*-$[Na_2Cl]GaS_2$, *t*-$[Na_2Cl]GaS_2$, *o*-$[Na_2Cl_{0.9}I_{0.1}]GaSe_2$, and *t*-$[Na_2Cl_{0.9}I_{0.1}]GaSe_2$.

compound	*d*(Cl–Na), Å	*d*(Ga–*Q*), Å
o-$[Na_2Cl]GaS_2$	2.7696(9) 2.7964(9) 2.8233(6) × 2 2.8286(6) × 2 2.7673(9) 2.7981(9) 2.8244(3) × 2 2.8274(3) × 2	2.2651(3) 2.2758(3) 2.2791(3) 2.2792(3) 2.2658(3) 2.2752(3) 2.2791(3) 2.2792(3)
t-$[Na_2Cl]GaS_2$	2.7697(13) 2.7958(12) 2.8225(8) × 2 2.8280(8) × 2	2.2642(5) 2.2757(4) 2.2779(4) × 2
o-$[Na_2Cl_{0.9}I_{0.1}]GaSe_2$	2.804(5) 2.872(5) 2.922(3) × 2 2.946(3) × 2 2.818(5) 2.876(5) 2.9321(12) × 2 2.9322(12) × 2	2.3859(10) 2.3860(10) 2.3969(8) 2.3973(10) 2.3893(11) 2.3939(8) 2.4019(10) 2.4020(10)
t-$[Na_2Cl_{0.9}I_{0.1}]GaSe_2$	2.813(3) 2.872(2) 2.922(2) × 2 2.937(2) × 2	2.3865(5) 2.3927(3) × 2 2.3955(5)

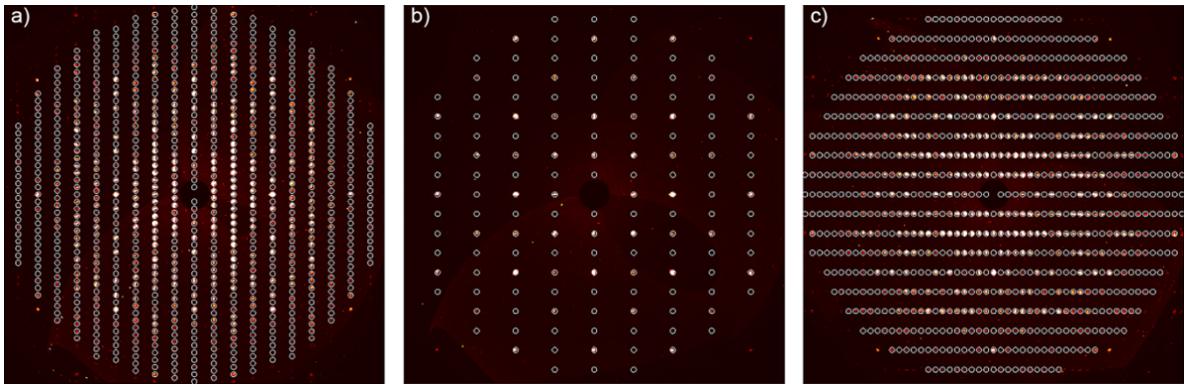

Figure S1. Precession image of (*a*) (*hk*0), (*b*) (*h*0*l*), and (*c*) (0*kl*) planes for *o*-$[Na_2Cl]GaS_2$ (s.g. *Cmcm*) single crystal. The simulated overlay is shown with white circles.

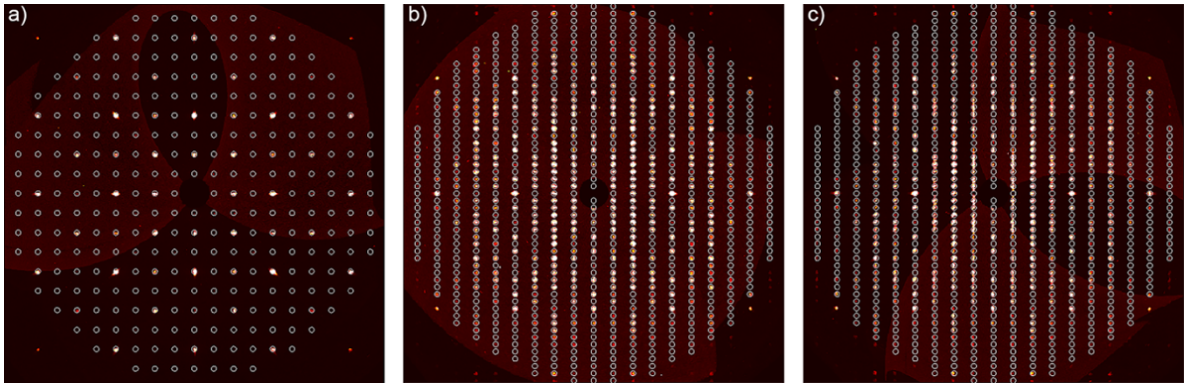

Figure S2. Precession image of (*a*) (*hk*0), (*b*) (*h*0*l*), and (*c*) (0*kl*) planes for *t*-[Na_2Cl]GaS_2 (s.g. *P*4_2*/nmc*) single crystal. The simulated overlay is shown with white circles.

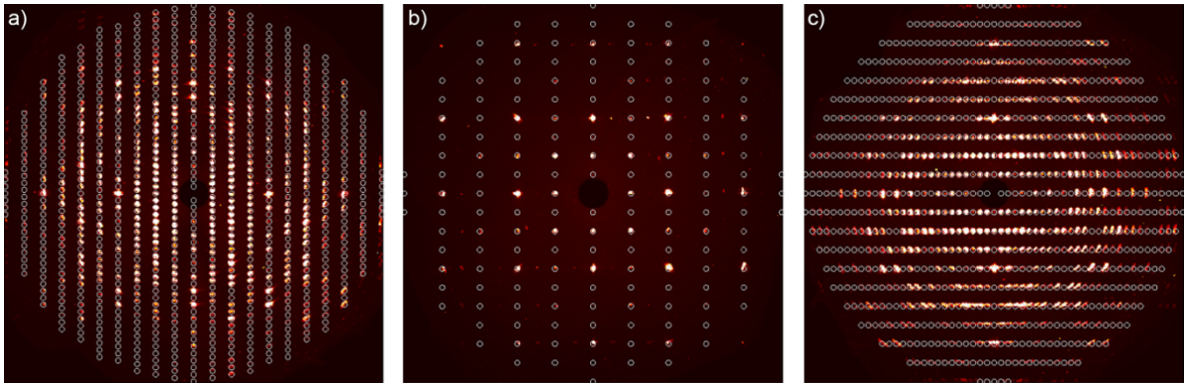

Figure S3. Precession image of (*a*) (*hk*0), (*b*) (*h*0*l*), and (*c*) (0*kl*) planes for *o*-[Na_2Cl]$GaSe_2$ (s.g. *Cmcm*) single crystal. The simulated overlay is shown with white circles.

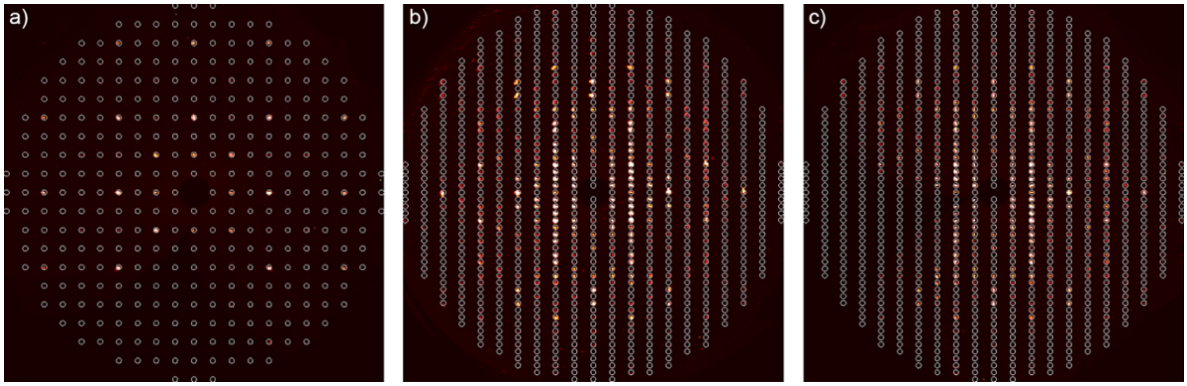

Figure S4. Precession image of (*a*) (*hk*0), (*b*) (*h*0*l*), and (*c*) (0*kl*) planes for *t*-[Na_2Cl]$GaSe_2$ (s.g. *P*4_2*/nmc*) single crystal. The simulated overlay is shown with white circles.

Table S3. EDS results for the single crystal of *o*-$[Na_2Cl]GaS_2$, *t*-$[Na_2Cl]GaS_2$, *o*-$[Na_2Cl_{0.9}I_{0.1}]GaSe_2$, *t*-$[Na_2Cl_{0.9}I_{0.1}]GaSe_2$, Na_2GaSe_3, and $Na_4Ga_2Se_5$.

o-$[Na_2Cl]GaS_2$	
element	atom %
Na	29.5(35)
Cl	17.5(5)
Ga	17.1(5)
S	35.9(5)

t-$[Na_2Cl]GaS_2$	
element	atom %
Na	34.3(19)
Cl	16.3(3)
Ga	15.3(3)
S	34.1(3)

o-$[Na_2Cl_{0.9}I_{0.1}]GaSe_2$	
element	atom %
Na	30.2(9)
Cl	21.7(6)
I	2.2(2)
Ga	14.9(19)
Se	31.0(29)

t-$[Na_2Cl_{0.9}I_{0.1}]GaSe_2$	
element	atom %
Na	31.0(7)
Cl	14.1(6)
I	2.1(4)
Ga	16.9(9)
Se	35.9(34)

Na_2GaSe_3	
Na	36.6(12)
Ga	14.8(4)
Se	48.6(11)

$Na_4Ga_2Se_5$	
Na	30.5(39)
Ga	18.9(4)
Se	50.6(9)

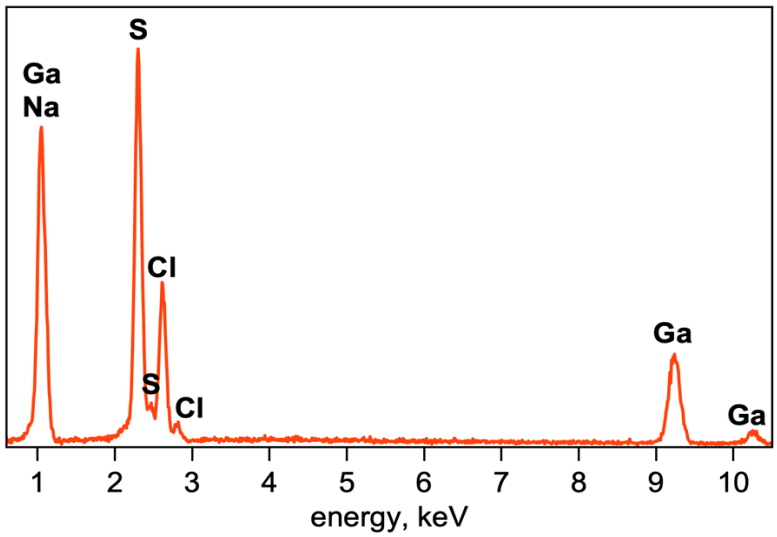

Figure S5. EDS spectra of *o*-$[Na_2Cl]GaS_2$.

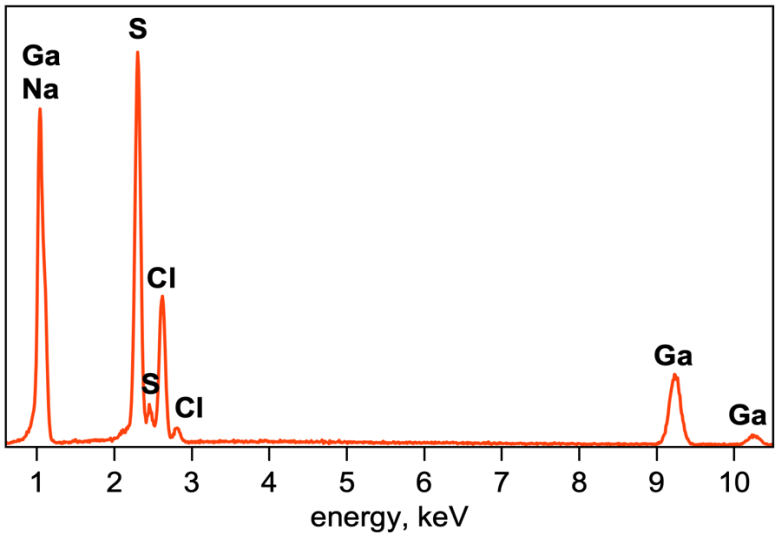

Figure S6. EDS spectra of *t*-[Na_2Cl]GaS_2.

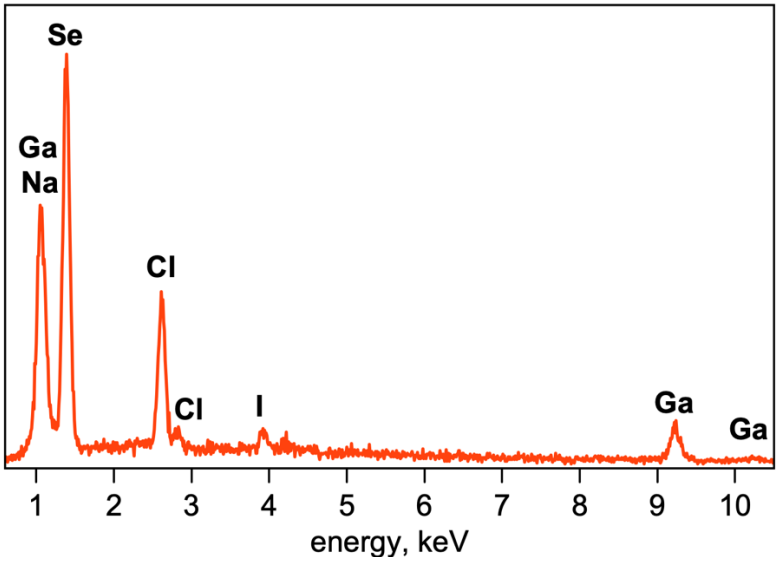

Figure S7. EDS spectra of *o*-[$Na_2Cl_{0.9}I_{0.1}$]$GaSe_2$.

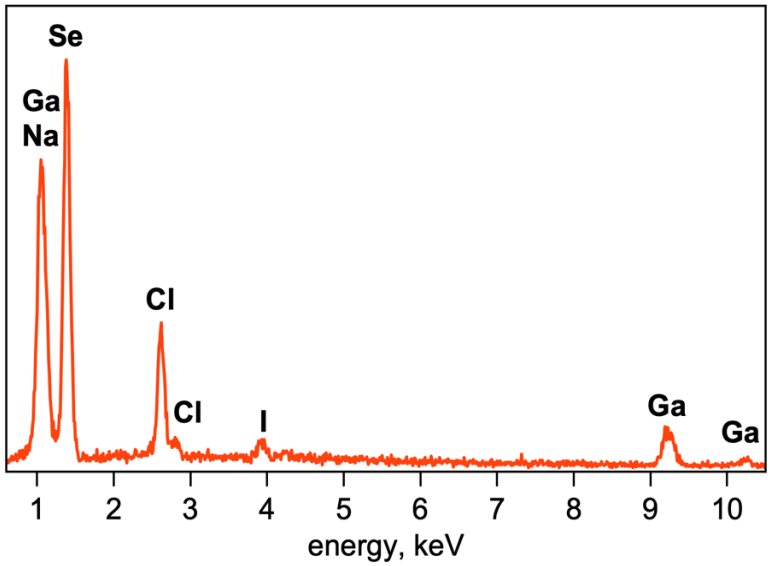

Figure S8. EDS spectra of *t*-[$Na_2Cl_{0.9}I_{0.1}$]$GaSe_2$.

Table S4. Crystallographic data for Na_2GaSe_3 and $Na_4Ga_2Se_5$.

compound	Na_2GaSe_3	$Na_4Ga_2Se_5$
empirical formula	Na_2GaSe_3	$Na_4Ga_2Se_5$
formula weight	352.58	626.2
temperature, K	299.61	298.93
crystal system	monoclinic	monoclinic
space group	$C2/c$	$P2_1/c$
a, Å	21.8190(4)	8.3169(3)
b, Å	8.3340(2)	6.4160(2)
c, Å	6.86160(10)	20.7332(7)
α, °	90	90
β, °	100.6730(10)	91.1838(13)
γ, °	90	90
volume, $Å^3$	1226.12(4)	1106.11(6)
Z	8	4
ρ_{calc}, g/cm^3	3.82	3.76
crystal size, mm^3	0.3 × 0.1 × 0.01	0.1 × 0.05 × 0.02
2Θ range for data collection, °	5.244 to 59.99	4.898 to 56.586
index ranges	$-30 \le h \le 30$, $-11 \le k \le 11$, $-9 \le l \le 9$	$-11 \le h \le 11$, $-8 \le k \le 8$, $-27 \le l \le 27$
reflections collected	24947	47434
data/restraints/ parameters	1798/0/57	2740/0/101
Goodness-of-fit on F^2	1.076	1.102
R_1/wR_2 [I>=2σ (I)], %	1.97/3.84	1.40/2.97
R_1/wR_2 [all data], %	2.63/4.18	1.71/3.10
largest diff. peak/hole, e $Å^{-3}$	0.70/–0.59	0.57/–0.70
R_{int}, %	6.18	6.41

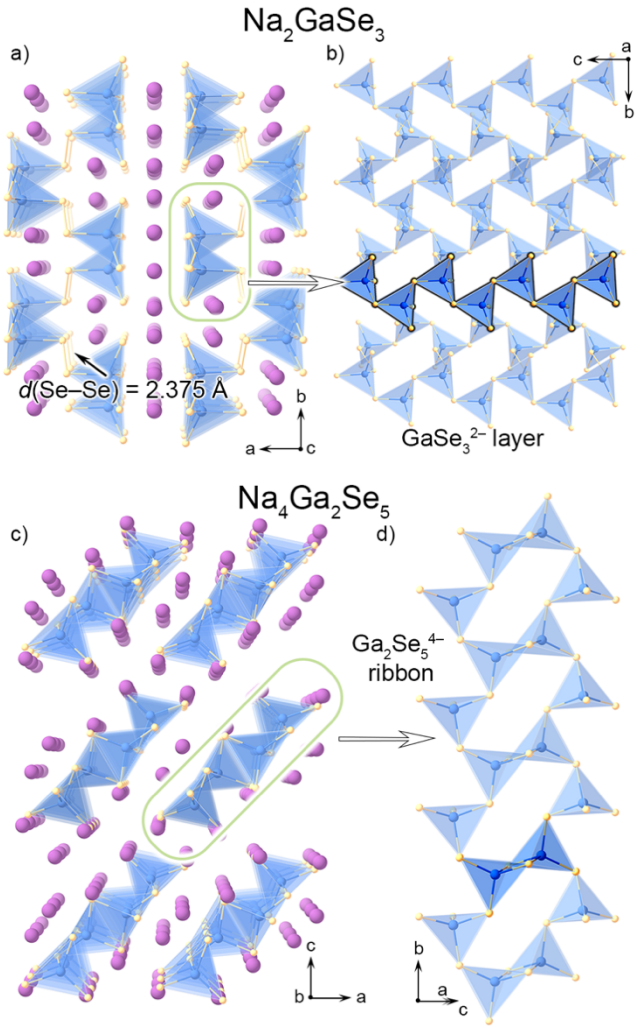

Figure S9. View of (*a*) Na_2GaSe_3 and (*c*) $Na_4Ga_2Se_5$ structures. Purple, blue, and yellow spheres and blue tetrahedra represent Na, Ga, and Se atom and $GaSe_4$ polyhedra, respectively. Na_2GaSe_3 structure consists of (*b*) the $GaSe_3^-$ layers that are built with (*b*) the corner-shared-$GaSe_4$ chains connected through (*a*) diselenides with a 2.375 Å Se–Se bond distance;[13] Na atoms are located between the $GaSe_3^{2-}$ layers and the chains. $Na_4Ga_2Se_5$ structure is isostructural to $Na_4Ga_2S_5$[14] and consists of (*d*) the $Ga_2Se_5^{4-}$ ribbons constructed through (*d*) the corner-sharing between $GaSe_4$ tetrahedra and the edge-sharing Ga_2Se_6 dimer; Na atoms fill the voids between the $Ga_2Se_5^{4-}$ ribbons.

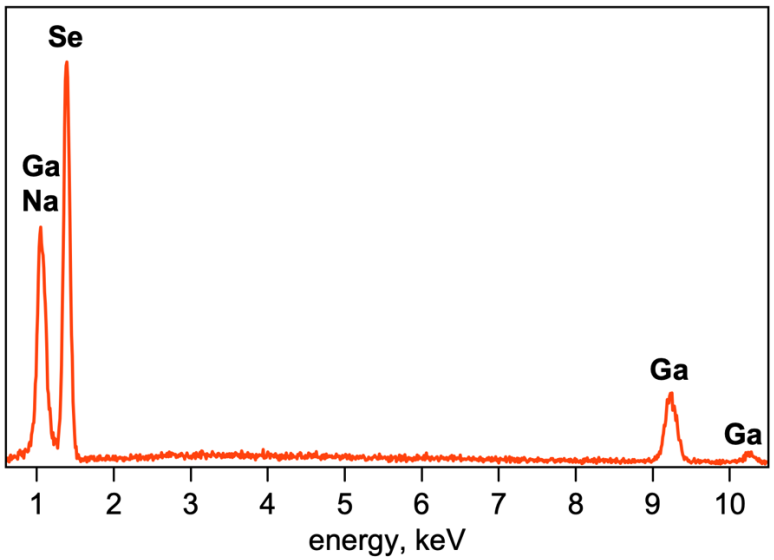

Figure S10. EDS spectra of Na_2GaSe_3.

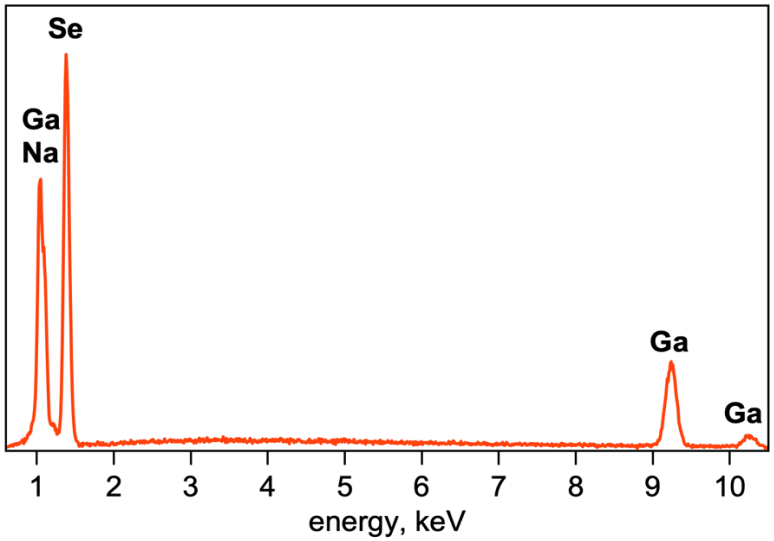

Figure S11. EDS spectra of $Na_4Ga_2Se_5$.

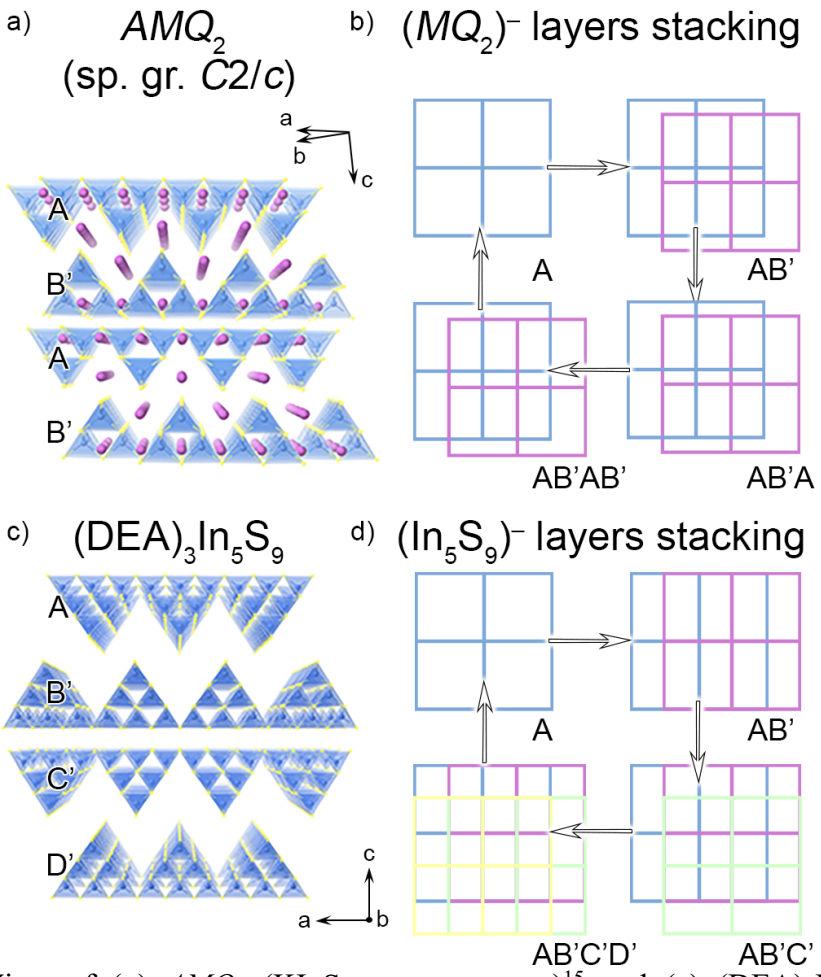

Figure S12. View of (*a*) AMQ_2 ($KInS_2$ structure type)[15] and (*c*) $(DEA)_3In_5S_9$ (DEA = diethylammonium)[16] structures. Purple, blue, and yellow spheres and blue tetrahedra represent *A*, *M* (Ga or In), *Q* atoms, and MQ_4 polyhedra, respectively. DEA ions were not determined from the SCXRD.[16] We analyzed the stacking motifs presented in the literature for the T_n-corner-sharing square net layers for the In and Ga chalcogenide-based materials,[17] and revealed only two stacking examples given in the literature: (*b*) A'B' in $KInS_2$ structure type and (*d*) A'B'C'D' for $(DEA)_3In_5S_9$ (DEA = diethylammonium) structure.[15, 16, 18] Blue, purple, green, and yellow square-net present unique T_n-corner-sharing layers where a node is a T_n supertetrahedral cluster. Both A'B' and A'B'C'D' stacking differ from the AB and ABCD stacking found for $[Na_2Cl]GaQ_2$ polymorphs (Figure 1). As DEA plays a template role in the $(DEA)_3In_5S_9$ structure formation, $ClNa_6$-based salt-inclusion templates novel stacking motifs for the GaS_2^- layers arrangement.

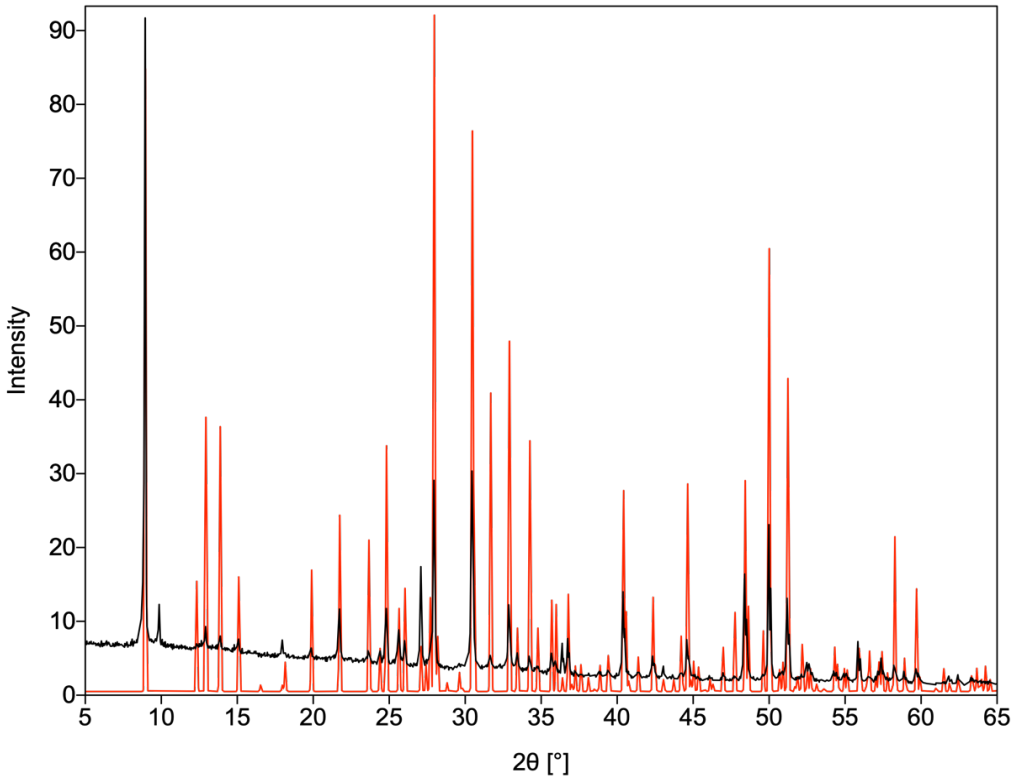

Figure S13. PXRD pattern for a product of reaction targeted $[Na_2Cl]GaS_2$ (black). Simulated pattern for *o*-$[Na_2Cl]GaS_2$ (red). Peak at 9.9° correspond to $NaGaS_2 \cdot H_2O$.[19]

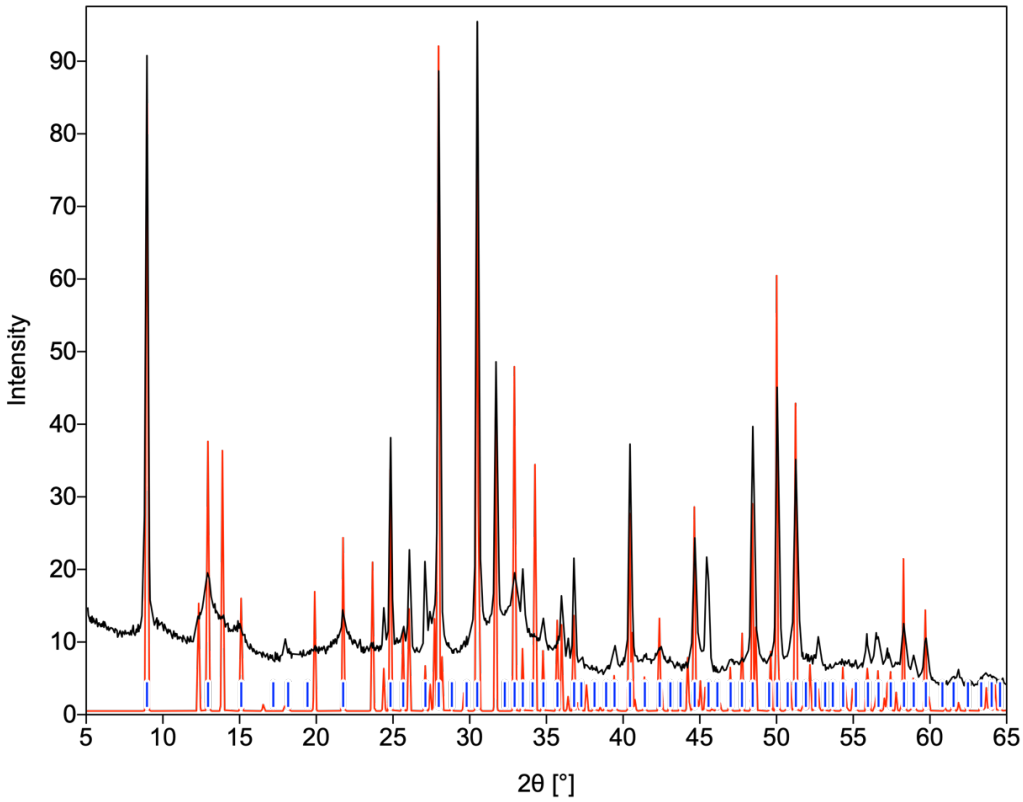

Figure S14. PXRD pattern of experimental $[Na_2Cl]GaS_2$ (black) and simulated *o*-$[Na_2Cl]GaS_2$ (red). Blue lines correspond to peak positions of the simulated *t*-$[Na_2Cl]GaS_2$ pattern.

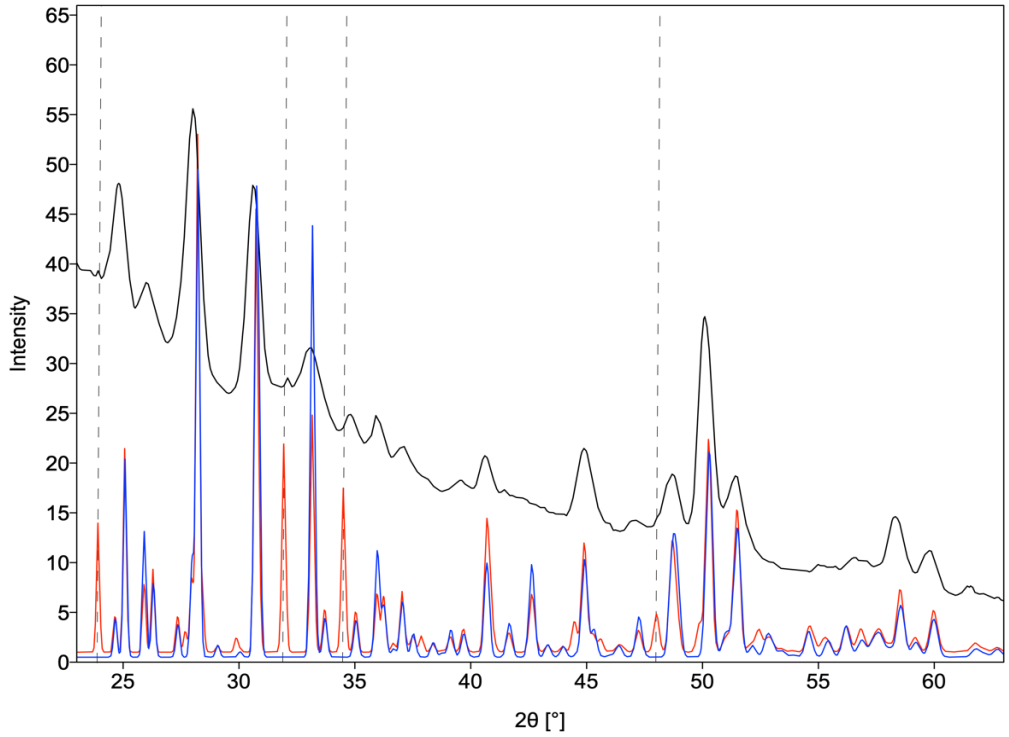

Figure S15. PXRD pattern of experimental *t*-[Na_2Cl]GaS_2 (black) and simulated *t*-[Na_2Cl]GaS_2 (blue) and *o*-[Na_2Cl]GaS_2 (red). Dash lines correspond to peak positions of the simulated *o*-[Na_2Cl]GaS_2 pattern that differ from the simulated *t*-[Na_2Cl]GaS_2 pattern.

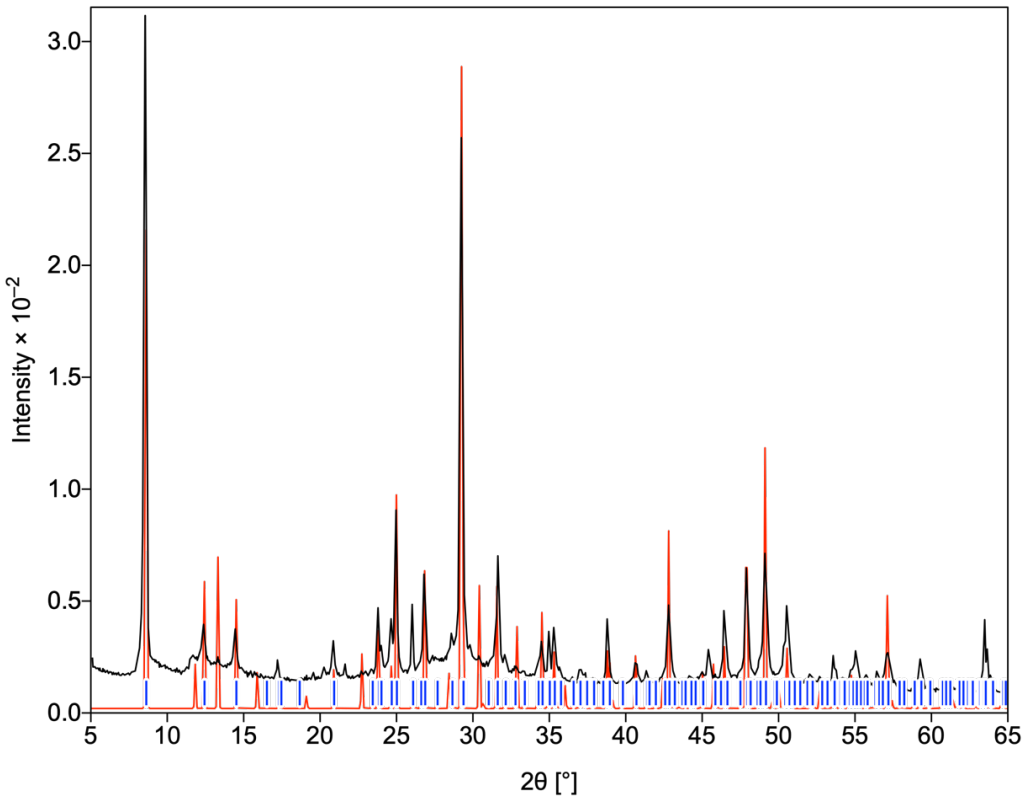

Figure S16. PXRD pattern of experimental [Na_2Cl]$GaSe_2$ (black) and simulated *o*-[Na_2Cl]$GaSe_2$ (red). Blue lines correspond to simulated t-[Na2Cl]GaSe2 pattern peak positions.

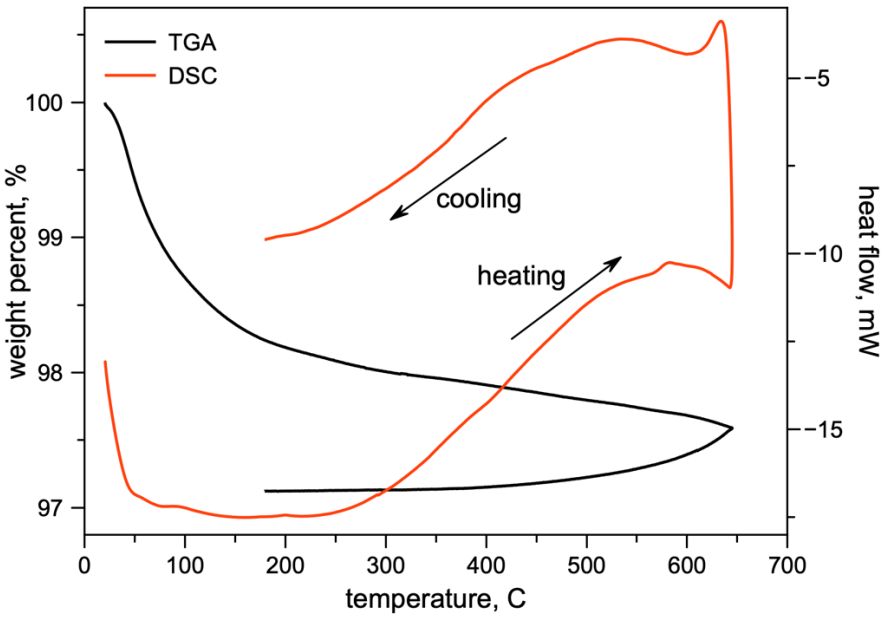

Figure S17. TGA(black)/DSC(red) plot of $[Na_2Cl]GaS_2$ in the 20–650 °C temperature range.

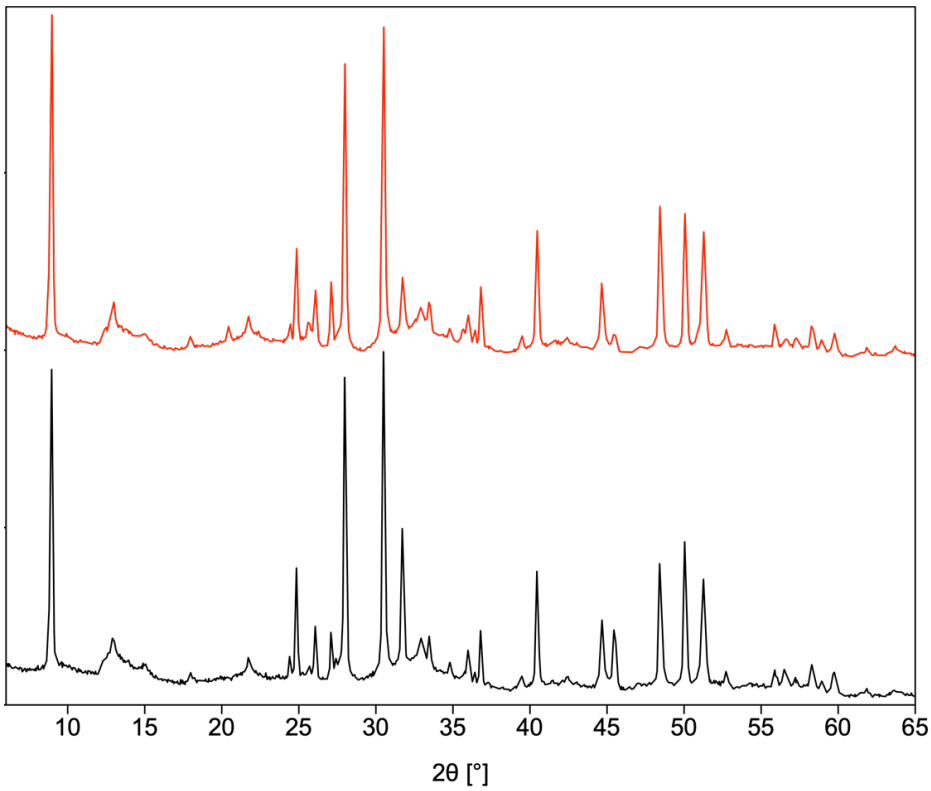

Figure S18. PXRD pattern of $[Na_2Cl]GaS_2$: before (black) and after TGA/DSC measurement in the 20–650 °C temperature range (red). A new peak at 20.4° can be seen in the post-heating sample.

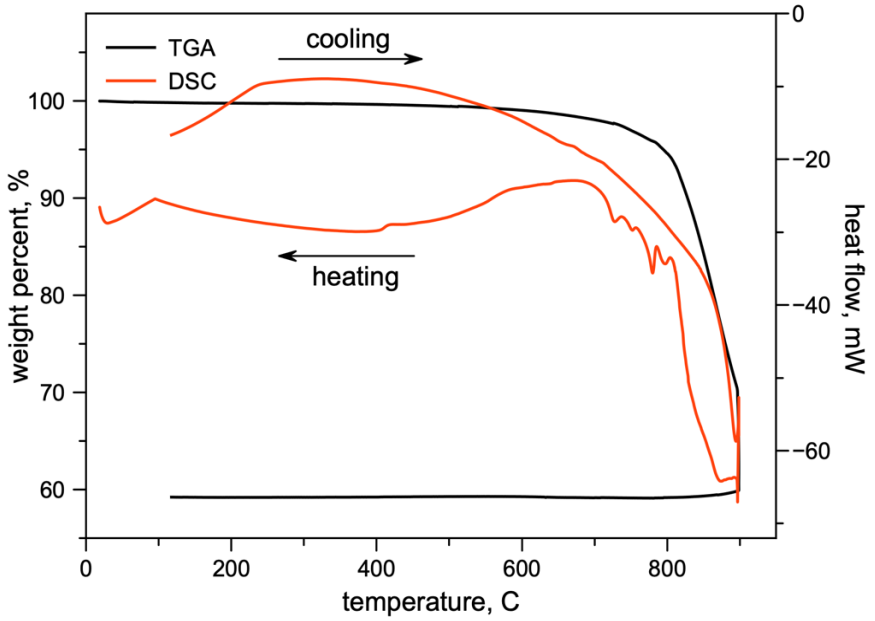

Figure S19. TGA(black)/DSC(red) plot of $[Na_2Cl]GaS_2$ in the 20–900 °C temperature range.

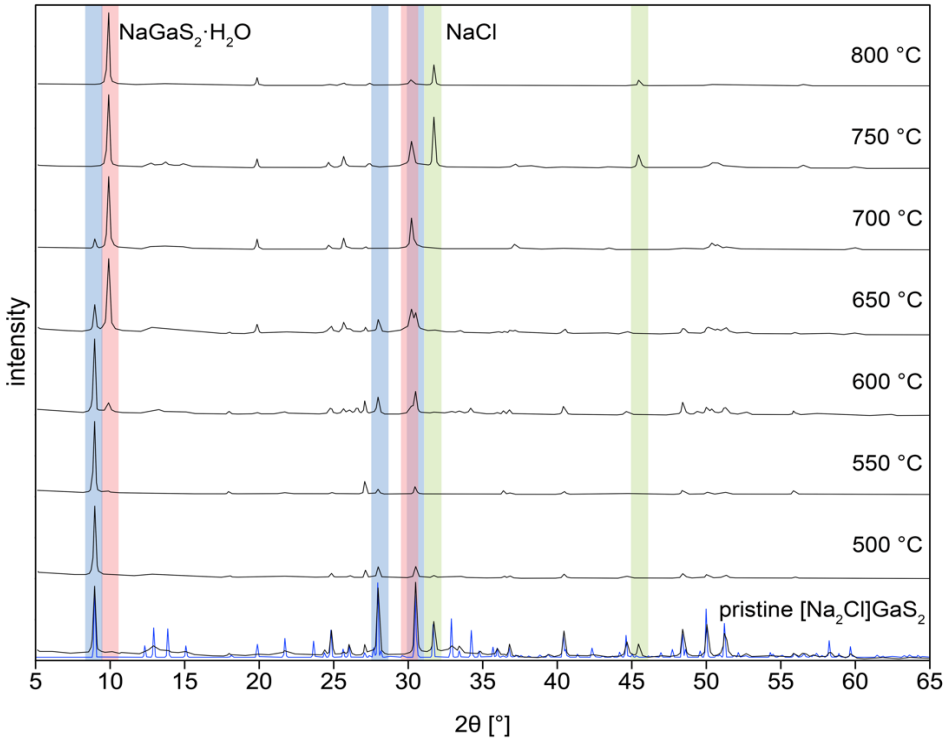

Figure S20. PXRD pattern for samples of the $[Na_2Cl]GaS_2$ annealed and quenched at different temperatures (black). Simulated pattern for *o*-$[Na_2Cl]GaS_2$ (blue). Blue, pink, and green box highlight the most intense peaks of $[Na_2Cl]GaS_2$, $NaGaS_2{\cdot}H_2O$, and NaCl phases, respectively.

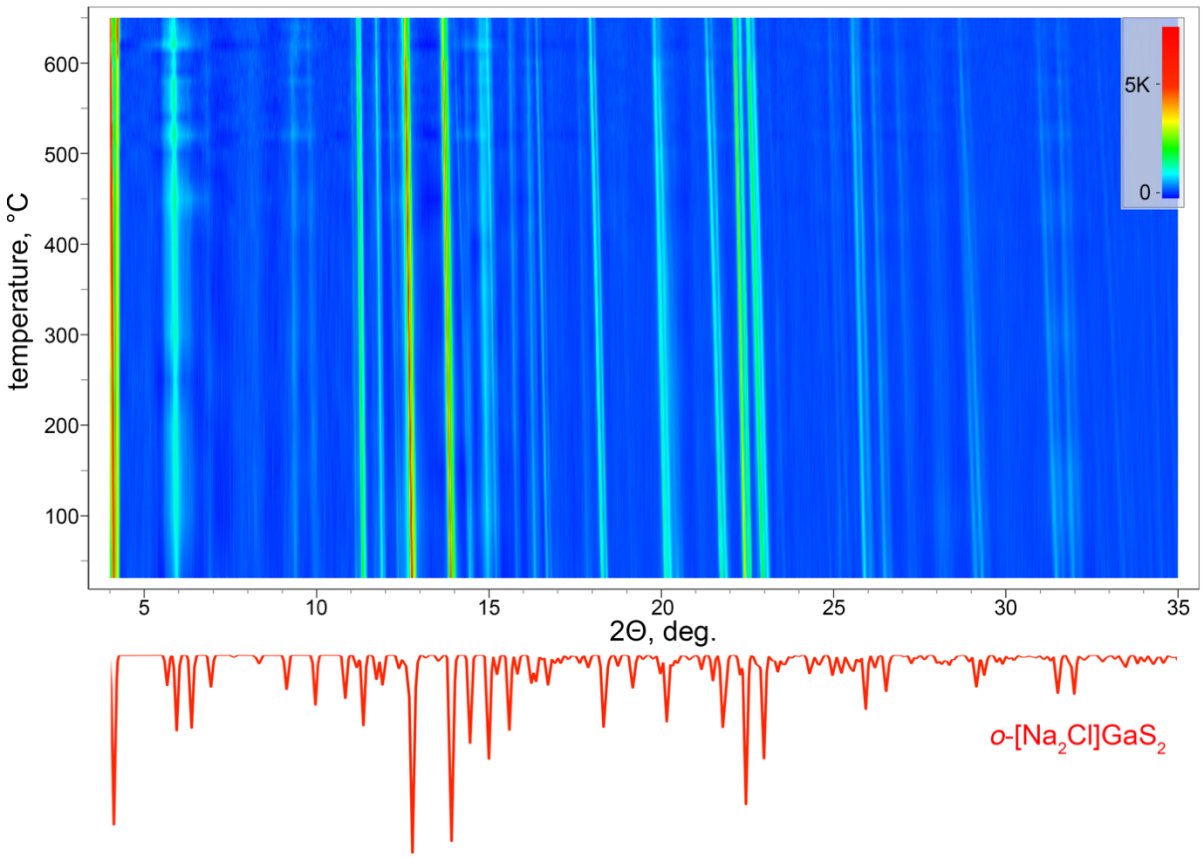

Figure S21. (*top*) Contour plot 2D image of the PXRD patterns for $[Na_2Cl]GaS_2$ in the sealed quartz glass capillary as a function of temperature. The HT-PXRD patterns were collected under Mo Kα irradiation. After 610 °C intensity of peaks corresponding to $[Na_2Cl]GaS_2$ reduces in comparison to the background, which may correlate with sample amorphization. The peak at ~4.1 ° is due to the capillary. (*bottom*) PXRD pattern of simulated *o*-$[Na_2Cl]GaS_2$ (red).

Table S5. DFT-calculated lattice constants,* enthalpies of formation at 0 K, and decomposition enthalpies for $[A_2X]GaS_2$ (A = Li, Na, and K; and X = F, Cl, and Br).

compound	*a*, Å	*b*, Å	*c*, Å	ΔH_f^{0K}, eV/atom	ΔH_{decom}^{0K}, kJ/mol
o-$[Na_2Cl]GaS_2$	7.37 (+1.1%)	39.78 (+0.9%)	7.37 (1.1%)	–1.41589	15.82
t-$[Na_2Cl]GaS_2$	7.37 (1.1%)		19.89 (+0.9%)	–1.41586	15.83
t-$[Na_2F]GaS_2$	7.20		19.04	–1.65	–24.9
t-$[Na_2Br]GaS_2$	7.48		20.27	–1.32	10.0
t-$[Li_2F]GaS_2$	7.06		17.35	–1.66	–101.8
t-$[Li_2Cl]GaS_2$	7.13		18.24	–1.36	–57.3
t-$[Li_2Br]GaS_2$	7.20		18.63	–1.27	–53.1
t-$[K_2F]GaS_2$	7.35		21.25	–1.72	–30.6
t-$[K_2Cl]GaS_2$	7.76		22.04	–1.45	–38.7
t-$[K_2Br]GaS_2$	7.90		22.57	–1.34	–57.5

* – The values within the parentheses indicate errors in the lattice constants with respect to the experimental values.

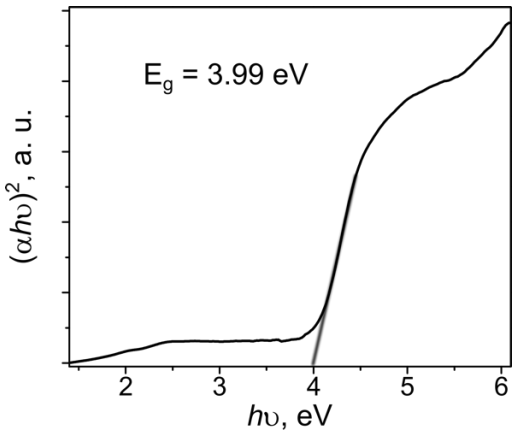

Figure S22. UV-vis spectra of $[Na_2Cl]GaS_2$.

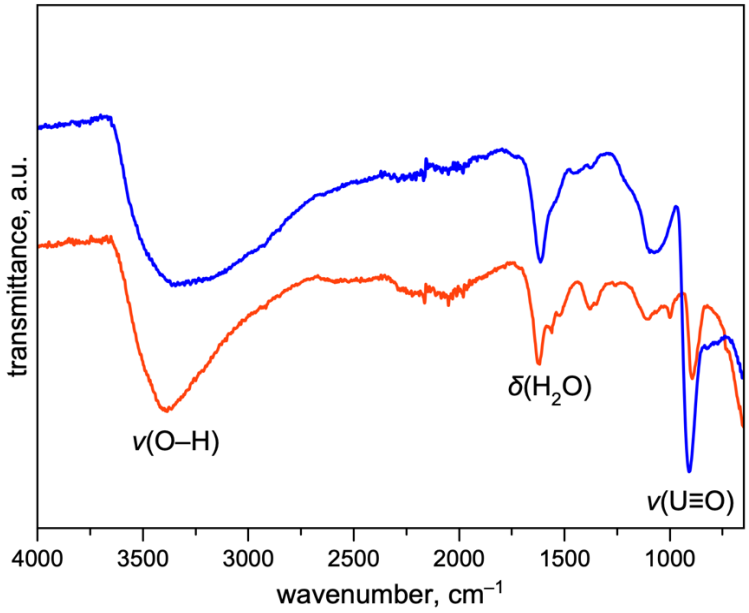

Figure S23. IR spectra of $[Na_2Cl]GaS_2$ after soaking in 0.001 M (red) and 0.01M (blue) UO_2^{2+} solution for 24 hours.

Table S6. EDS results for the single crystal of $[Na_2Cl]GaS_2$ soaked in 0.01 M UO_2^{2+} solution for 3 and 24 hours.

$[Na_2Cl]GaS_2$ (3h)_1	
element	atom %
Na	34.6(21)
Cl	15.9(12)
Ga	16.4(17)
S	32.8(13)
U	0.3(2)

$[Na_2Cl]GaS_2$ (3h)_2	
element	atom %
Na	22.1(17)
Cl	8.6(7)
Ga	28.9(29)
S	36.6(17)
U	3.8(7)

$[Na_2Cl]GaS_2$ (24h)	
element	atom %
Na	0
Cl	1.0(5)
Ga	49(4)
S	24.4(13)
U	25.6(10)

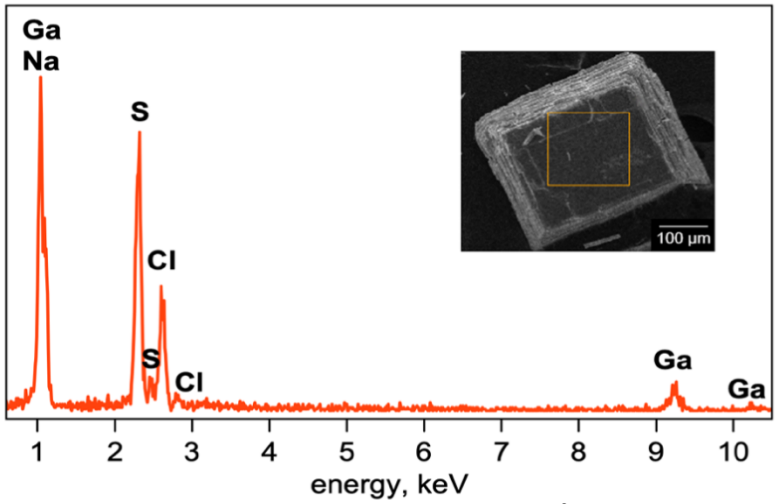

Figure S24. EDS spectra of $[Na_2Cl]GaS_2$ soaked in 0.01 M UO_2^{2+} solution for 3 hours. The insert shows the area chosen for EDS analysis.

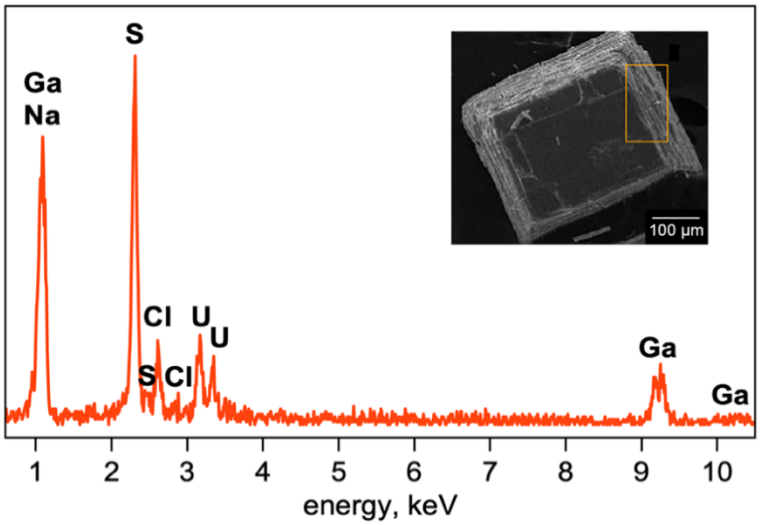

Figure S25. EDS spectra of $[Na_2Cl]GaS_2$ soaked in 0.01 M UO_2^{2+} solution for 3 hours. The insert shows the area chosen for EDS analysis.

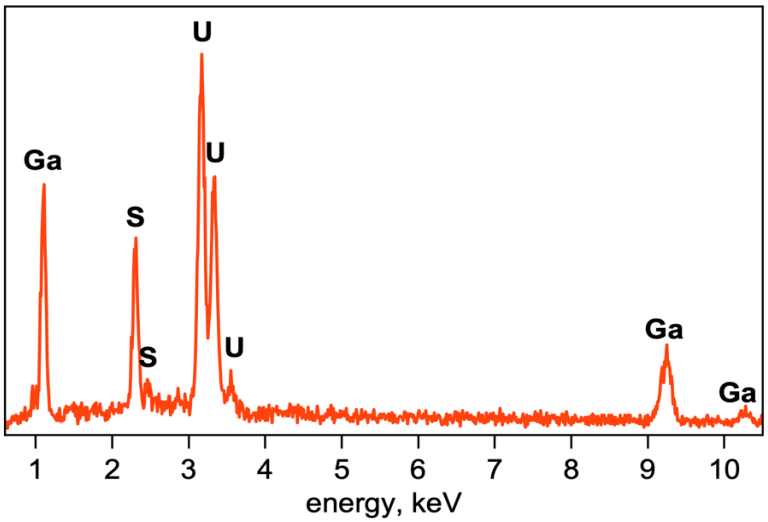

Figure S26. EDS spectra of $[Na_2Cl]GaS_2$ soaked in 0.01 M UO_2^{2+} solution for 24 hours.

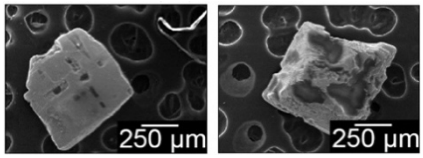

Figure S27. SEM images of $[Na_2Cl]GaS_2$ single crystals in UO_2^{2+} solution.

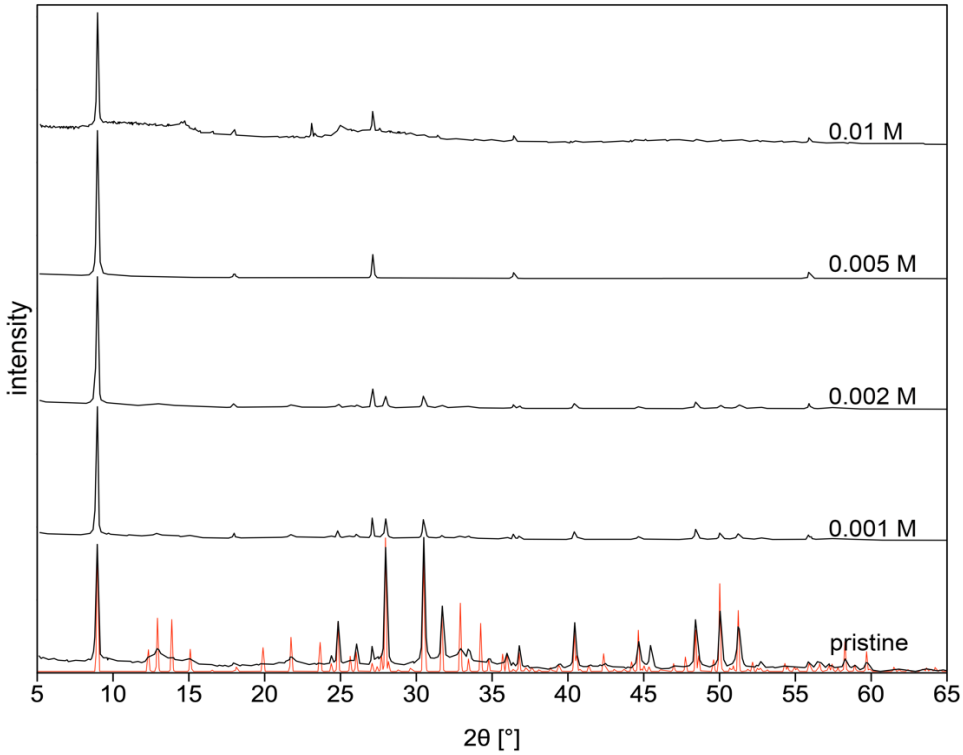

Figure S28. PXRD pattern for samples of the $[Na_2Cl]GaS_2$ single crystals soaked in UO_2^{2+} solution for 24 hours (black). Simulated pattern for *o*-$[Na_2Cl]GaS_2$ (red).

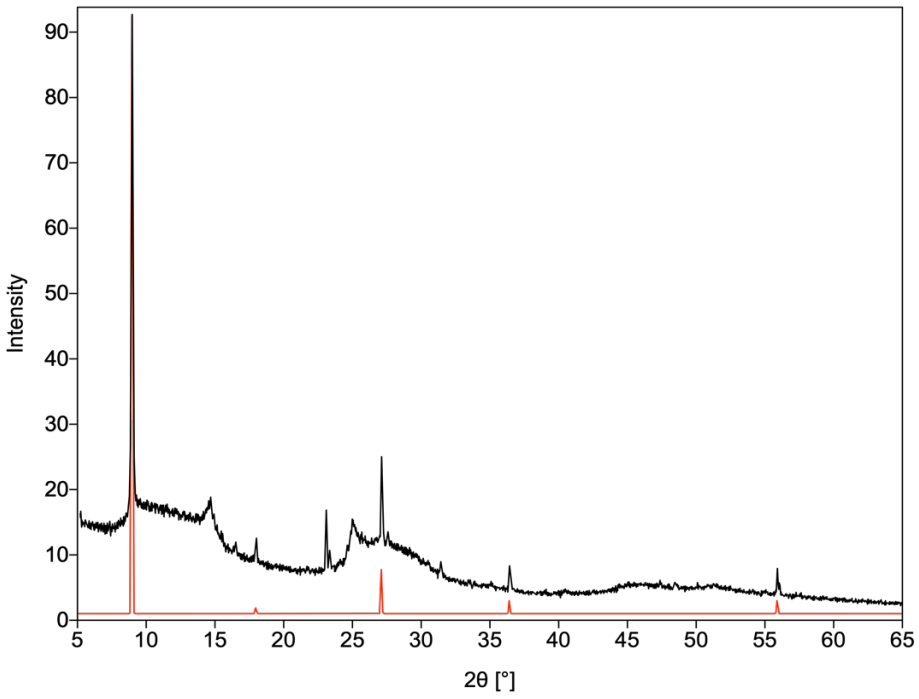

Figure S29. PXRD pattern for samples of the $[Na_2Cl]GaS_2$ single crystals soaked in 0.01 M UO_2^{2+} solution for 24 hours (black). Simulated pattern for *o*-$[Na_2Cl]GaS_2$ with the preferred orientation along [040] (red). We were not able to assign peaks at 14.6°, 23.0°, 23.4°, and 27.6 ° to a specific phase. From the literature analysis of reports on uranyl exchange with layered chalcogenides, we found an example of reversible uranyl species intercalation between layers for $K_2MnSn_2S_6$ (KMS-1)[20] material. In KMS-1, Potassium ions were substituted by $UO_2^{2+,}$ which resulted in an interlayer distance shrinkage from 8.5 Å to 7.4 Å. In the case of $[Na_2Cl]GaS_2$ material, the distance between GaS_2^- layers is significantly higher (9.9 Å vs. 8.5 Å), and uranyl species integration is likely to start structure degradation decomposition and results in an amorphous product.

References

(1) Krause, L.; Herbst-Irmer, R.; Sheldrick, G. M.; Stalke, D. Comparison of Silver and Molybdenum Microfocus X-ray Sources for Single-Crystal Structure Determination. *J. Appl. Crystallogr.* **2015**, *48*, 3-10.

(2) Bruker (2012). SAINT. Bruker AXS Inc., Madison, Wisconsin, USA.

(3) Dolomanov, O. V.; Bourhis, L. J.; Gildea, R. J.; Howard, J. A. K.; Puschmann, H. *OLEX2*: a Complete Structure Solution, Refinement and Analysis Program. *J. Appl. Crystallogr.* **2009**, *42*, 339-341.

(4) Sheldrick, G. M. Crystal Structure Refinement with SHELXL. *Acta Cryst.* **2015**, *71*, 3-8.

(5) Kresse, G.; Furthmüller, J. Efficiency of *ab-initio* Total Energy Calculations for Metals and Semiconductors Using a Llane-Wave Basis Set. *Comput. Mater. Sci.* **1996**, *6*, 15-50.

(6) Kresse; Furthmüller. Efficient Iterative Schemes for *ab initio* Total-Energy Calculations Using a Plane-Wave Basis Set. *Phys. Rev. B: Condens. Matter Mater. Phys.* **1996**, *54*, 11169-11186.

(7) Kresse, G.; Joubert, D. From Ultrasoft Pseudopotentials to the Projector Augmented-wave Method. *Phys. Rev. B: Condens. Matter Mater. Phys.* **1999**, *59*, 1758-1775.

(8) Perdew; Burke; Ernzerhof. Generalized Gradient Approximation Made Simple. *Phys. Rev. Lett.* **1996**, *77*, 3865-3868.

(9) Kirklin, S.; Saal, J. E.; Meredig, B.; Thompson, A.; Doak, J. W.; Aykol, M.; Rühl, S.; Wolverton, C. The Open Quantum Materials Database (OQMD): Assessing the Accuracy of DFT Formation Energies. *npj Comput. Mater.* **2015**, *1*, 15010.

(10) Saal, J. E.; Kirklin, S.; Aykol, M.; Meredig, B.; Wolverton, C. Materials Design and Discovery with High-Throughput Density Functional Theory: The Open Quantum Materials Database (OQMD). *JOM* **2013**, *65*, 1501-1509.

(11) Bergstrom, F. W. The Polysulfides and Polyselenides of Lithium, Sodium and Potassium. *J. Am. Chem. Soc.* **1926**, *48*, 146-151.

(12) Balijapelly, S.; Sundaramoorthy, S.; Mondal, D. J.; Konar, S.; Gerasimchuk, N.; Chernatynskiy, A.; Choudhury, A. $NaGaSe_2$: A Water-Loving Multifunctional Non-van der Waals Layered Selenogallate. *Inorg. Chem.* **2023**, *62*, 3886-3895.

(13) Graf, C.; Assoud, A.; Mayasree, O.; Kleinke, H. Solid State Polyselenides and Polytellurides: A Large Variety of Se–Se and Te–Te Interactions. *Molecules* **2009**, *14*, 3115-3131.

(14) Klepp, K. O. Preparation and Crystal Structure of $Na_4Ga_2S_5$. A Thiogallate with --zweier-Double Chains. *Z. Naturforsch.* **1992**, *47*, 937-941.

(15) Eisenmann, B.; Hofmann, A. Crystal Structure of Potassium Phyllo-dithioindate(III), $KInS_2$. *Z. Kristallogr.* **1991**, *195*, 318-320.

(16) Cahill, C. L.; Parise, J. B. On the Formation of Framework Indium Sulfides. *J. Chem. Soc., Dalton Trans.* **2000**, 1475-1482.

(17) Sun, M.; Zhang, S.; Wang, K.-Y.; Wang, J.; Cheng, L.; Zhu, J.-Y.; Zhao, Y.-M.; Wang, C. Mixed Solvothermal Synthesis of T_n Cluster-Based Indium and Gallium Sulfides Using Versatile Ammonia or Amine Structure-Directing Agents. *Inorg. Chem.* **2021**, *60*, 7115-7127.

(18) Zhou, J.; Zhang, Y.; Bian, G.-Q.; Li, C.-Y.; Chen, X.-X.; Dai, J. Structural Study of Organic−Inorganic Hybrid Thiogallates and Selenidogallates in View of Effects of the Chelate Amines. *Cryst. Growth Des.* **2008**, *8*, 2235-2240.

(19) Klepov, V. V.; Berseneva, A. A.; Pace, K. A.; Kocevski, V.; Sun, M.; Qiu, P.; Wang, H.; Chen, F.; Besmann, T. M.; zur Loye, H. $NaGaS_2$: An Elusive Layered Compound

with Dynamic Water Absorption and Wide-Ranging Ion-Exchange Properties. *Angew. Chem.* **2020**, *132*, 10928-10933.
(20) Manos, M. J.; Kanatzidis, M. G. Layered Metal Sulfides Capture Uranium from Seawater. *J. Am. Chem. Soc.* **2012**, *134*, 16441-16446.